Optical study of defects in lithium iodate α-$LiIO_3$

Alexander P. Yelisseyev,* Ludmila I. Isaenko, and Marina K. Starikova

Sobolev Institute of Geology and Mineralogy, Siberian Branch of the Russian Academy of Sciences, 3 Academician Koptyug Avenue, 630090, Novosibirsk, Russia
**Corresponding author: eliseev.ap@mail.ru*

Received December 8, 2011; accepted March 21, 2012;
posted April 18, 2012 (Doc. ID 158826); published May 25, 2012

Photoluminescence (PL) in two broad bands at 2.95 and 2.6 eV in lithium iodate α-$LiIO_3$ is associated with self-trapped excitons and native point defects (supposedly oxygen vacancies), respectively, based on the luminescence excitation spectra and the PL temperature dependence. Free charge carriers may be captured by two types of shallow traps with thermal activation energies of 0.14 and 0.21 eV: they are responsible for crystal darkening at temperatures below 200 K. Spontaneous emission of α-$LiIO_3$ during cooling or heating at temperatures $T < 200$ K is pyroluminescence, which occurs at dielectric breakdown in strong pyroelectric fields on the crystal surface and in its bulk as well as inside the channel defects.

OCIS codes: 300.1030, 300.6250, 300.6280.

1. INTRODUCTION

Three modifications of lithium iodate $LiIO_3$ exist in the solid state: orthorhombic γ, tetragonal β, and hexagonal α [1–4]. Of them, only the α phase is nonsymmetric (point group 6) and demonstrates strongly pronounced piezoelectric, nonlinear, ferroelectric, and pyroelectric properties. This crystal is used in optoelectronic and quantum electronic devices [1–4]: α-$LiIO_3$ is a negative uniaxial crystal with $n_o > n_e$, pyroelectric. Its second-order nonlinear susceptibility $d_{31}(1.06\ \mu m) = 4.1$ pm/V is higher than that of KTP [2]. Crystal is grown from aqueous solutions, and it is hygroscopic, but this problem is solved by coating the crystal surface. Crystals for quantum electronics should be of high optical quality, which is determined by point and extended defects inside. Most papers concerning α-$LiIO_3$ have been devoted to the study of extended defects and the formation conditions and the physical and chemical properties of crystals and their applications [1–4]. The extended defects under consideration have been dislocations, growth sectors, inclusions, and channel defects [1,4–6]. Practically nothing is known about point defects in α-$LiIO_3$ and radiative processes with their participation. The aim of this paper is to study the point defects participating in the α-$LiIO_3$ luminescence as well as unusual spontaneous emission of this crystal during its heating or cooling: such emission is known as pyroelectric luminescence (PEL) [7,8].

2. EXPERIMENTAL SECTION

A. Structure and Growth of α-$LiIO_3$ Crystals

Crystals of α-$LiIO_3$ were grown at room temperature by slow and controlled evaporation of slightly supersaturated aqueous solutions, and the most stable polar hexagonal α phase is crystallized in such conditions. In the α-$LiIO_3$ lattice, the oxygen atoms form a dense packing with slightly distorted oxygen octahedrons. The density of the hexagonal packing of oxygen atoms in α-$LiIO_3$ is 52%. The iodine atoms occupy octahedral cavities so that I^{5+} is more strongly bound to three of six oxygen ions in the octahedron, thus forming a group of C_3 symmetry [1,3]. Namely, the existence of such a polar group determines the nonlinear properties of α lithium iodate. The Li^+ ions also occupy the octahedral positions and form the chains parallel to the six axes. At 570 K, the irreversible transition to the tetrahedral β phase takes place [3]. The existence of intermediate γ phase, which forestalls the $\alpha \rightarrow \beta$ transition, is possible [1,3]. We studied mainly "neutral" crystals with higher pH values (pH~7) relative to "acid" samples (pH~2.5), which include some HIO_3. The "neutral" crystals are known to be lighter and highly transparent (with transparency up to T~80%) in the 0.32 to 5 μm range, whereas the "acid" α-$LiIO_3$ samples have a 0.34 μm (3.6 eV) absorption band and are yellowish [1]. Such "neutral" crystals were used to produce nonlinear α-$LiIO_3$ optical elements. The sizes of grown crystals α-$LiIO_3$ were up to 10 cm. Afterward, we prepared the polished (100) and (001) plates ~2 mm thick, with aperture ~0.5 cm^2 for spectroscopic measurements. The side faces of the (100) plates were parallel or perpendicular to the optical axis $\boldsymbol{c}$.

B. Spectroscopic Study

Transmission spectra in the transparency range of α-$LiIO_3$ were recorded using a Shimadzu 2501 and IR Fourier transform Infralum 801 spectrometers. The photoluminescence (PL) spectra were recorded using the SDL1 spectrometer with excitation in the Hg lines from the DRSh100/2 lamp. The photoluminescence excitation (PLE) spectra were obtained scanning the light of a 1 kW Xe lamp through the MDR2 monochromator, whereas PL wavelength was selected using the SDL1 spectrometer or an appropriate glass filter. When measuring the temperature dependencies, a crystal was placed inside a vacuum metal liquid nitrogen cryostat with silica windows.

Absorption coefficients were calculated from transmission measurements in the transparency region by use of the following formula [9]:

$$T = ((1-R)^2 e^{-\alpha d})/(1-R^2 e^{-2\alpha d}), \quad (1)$$

where α is the absorption coefficient (cm^{-1}), d is the sample thickness (in centimeters), and R is the reflection coefficient

per one surface. Here we took into account the multiple reflections when a beam passes through the polished crystal. The R values measured using a technique of minimum deviation angle and the Sellmeier equations for the $R(\lambda)$ approximation were taken from [2]. The thermoluminescence (TL) curves were recorded when heating a sample at a rate of $\beta = 0.2$ K/s after preliminary illumination over 10 min at a low temperature (80 K).

3. RESULTS AND DISCUSSION

A. Transmission Spectra

Transmission spectra recorded in polarized light for 2 mm thick α-$LiIO_3$ samples are shown in Fig. 1. The shortwave transmission edge on the 50% transmission level is 4.32 and 4.206 eV at room temperature for ordinary and extraordinary beams, respectively. In the mid-IR, we also showed the unpolarized spectrum for a 34 mm long α-$LiIO_3$ sample (curve 3) for comparison. The absorption spectrum calculated using Eq. (1) is given in Fig. 2 for $E \perp c$ and $E \| c$ polarizations (curves 3 and 4, respectively). The type of electronic transitions responsible for band-to-band transitions was identified based on the analysis of the shape of the fundamental absorption edge [10]. The absorption spectra for α-$LiIO_3$ become a straight line in the $(\alpha h\nu)^2 = f(h\nu)$ coordinates, which means that there are direct allowed electronic transitions [10]. The bandgap value E_g was determined as a cross point where an extrapolated linear part of the absorption curve intersects the abscissa axis. At room temperature, we obtained $E_g = 4.38$ and 4.415 eV for ordinary and extraordinary beams, respectively. This is in accord with $E_g = 4.37$эВ [11], but it considerably exceeds the 4.0 eV value from [12]. The longwave transparency edge at $\lambda > 9$ μm and an intense absorption band near 6 μm are determined by the two-phonon transition in the matrix [13]. The transparency worsening takes place in the 0.28 to 0.4 and 2.7 to 4.4 μm ranges: it depends on the purity of the reagents, seed quality, and growth regime [1,14]. This absorption is stronger in "acid" α-$LiIO_3$ crystals and is negligible in "neutral" samples. The 2.7 to 3.5 μm absorption is associated with the vibrations of O—H groups in HIO_3 or HI_3O_8 when they are added during growth. The 4.3 μm band is due to valent vibrations of the I—O bond [1]. Maximum absorption intensity is observed in the $E \perp c$ polarization (Fig. 1).

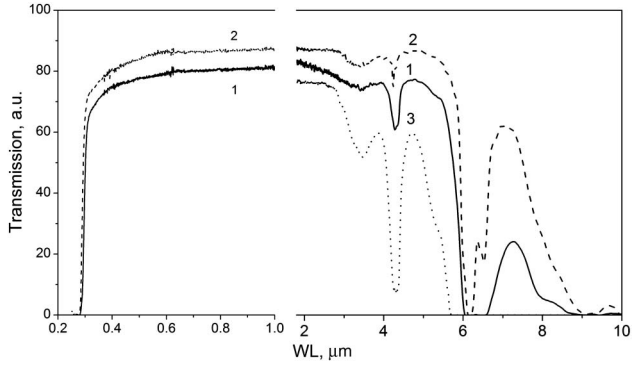

Fig. 1. Transmission spectra of α-$LiIO_3$ for a 2 mm thick plate recorded in polarized light: for $E \perp c$ (curve 1) and $E \| c$ (curve 2). The unpolarized transmission spectrum of the 34 mm long sample (curve 3) is given for comparison. $T = 300$ K.

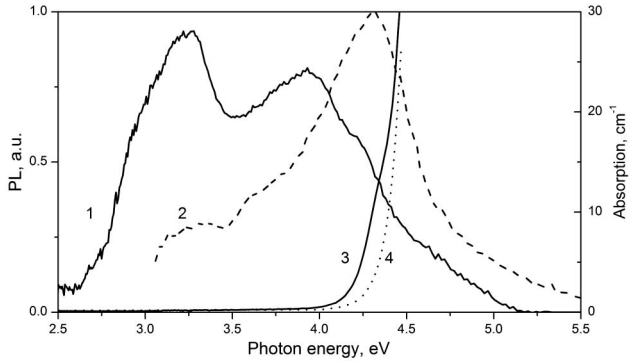

Fig. 2. PLE spectra for 2.25 eV (550 nm, curve 1) and 2.89эВ (430 nm, curve 2) PL emissions, recorded at 300 and 80 K, respectively. Spectra 3 and 4 are absorption spectra for ordinary and extraordinary beams at 300 K.

B. Photoluminescence

The α-$LiIO_3$ crystals have a weak white–bluish PL at UV excitation. PL spectra recorded at 80, 300, 400, and 500 K are given in Fig. 3. Above room temperature, there is the only broad band centered at 2.6 eV (480 nm) with the full-width at half-maximum (FWHM) = 0.74 eV. This PL emission quenches slowly as the temperature increases from 80 K to 500 K, whereas the PL band maximum shifts to 2.3 eV (Fig. 3). Below 250 K, there is another narrower band centered at 2.95 eV (420 nm), with the FWHM = 0.1 eV. The considerable width of the PL bands, even at the liquid helium temperature, shows a strong electron–phonon interaction in this crystal. In such a case, the band shape is close to Gaussian. The results of PL decomposition into Gauss components are shown by thin black solid lines in Fig. 3.

The band 2.6 eV emission is more intense in defect areas of the samples, near cracks and inclusions, and seems to be related to some native point defects. We found also that its intensity increases several times after crystal annealing at 300–400 K during 2 to 3 h in vacuum: thus, this PL may be preliminarily associated with anion (oxygen) vacancies. On the other hand, PL approximately at the same photon energies was found in some other oxides such as Al_2O_3 [15].

The low-temperature 2.95 eV PL is excited most effectively at short wavelengths: one can see a broad band with maximum at 4.3 eV in the PLE spectra (Fig. 2, curve 2). It is a region where

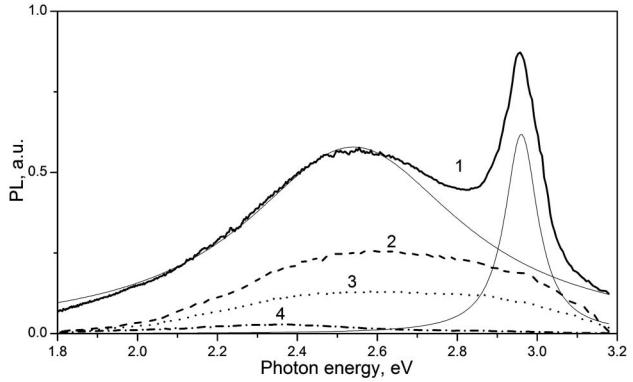

Fig. 3. PL spectra of α-$LiIO_3$ at 3.37 eV excitation, recorded at 80, 300, 400, and 500 K (curves 1–4, respectively). Thin solid lines show the results of spectrum 1 decomposition into Gaussian components.

the absorption coefficient increases rapidly as a result of band-to-band electronic transitions (curves 3, 4). Such absorption/PLE bands near the fundamental edge are usually of excitonic origin [16]. PL in the 2.6 eV band is excited in two broad bands at 3.25 and 3.95 eV in the α-$LiIO_3$ transparency range (Fig. 2). These two bands correspond to electronic transitions from the ground state of the defects to their excited state (3.25 eV) and to the conduction band (3.95 eV). The concentration of the corresponding defects is rather low, and we do not see corresponding bands in the absorption spectra of α-$LiIO_3$.

C. Temperature Dependence of Photoluminescence

The temperature dependence of the intensity in the 2 to 3 eV range is given in Fig. 4. PL quenches in the 80 to 550 K range in two steps, and this process is described well by the Mott law [8]. In this case, the PL quantum yield corresponds to the following equation [10]:

$$\eta(T) \propto [1 + \tau_R \nu_0 \exp(-\Delta E/kT)]^{-1}, \quad (2)$$

where τ_R is a radiative lifetime at low temperature (s), ΔE is an energy barrier (eV) for exit to the radiationless channel, and ν_0 is the jump frequency (s^{-1}). The quenching of PL with increasing temperature is explained as an activation of electronic transitions from the excited to the ground state with further nonradiative relaxation [10]. An experimental temperature dependence of PL for integral emission in Fig. 4 demonstrates two well-pronounced quenching ranges: 120 to 250 K and 350 to 550 K. Dotted curves 3 and 4 are the results of calculating according to (2) in these two ranges, whereas curve 2 shows their sum. The fitting parameters are the following: 4×10^4 and 2×10^4 for pre-exponential factors and 0.18 and 0.42 eV for thermal activation energies for curves 3 and 4, respectively. These two stages correspond to quenching PL in the 2.95 and 2.6 eV bands, respectively.

PL in the 2.6 eV band corresponding to intracenter radiative transitions quenches rather slowly. The low-temperature PL in the 2.95 eV excited near the fundamental absorption edge, with a large Stokes shift exceeding 1 eV and fast temperature quenching, may be due to the recombination of self-trapped excitons (STEs) [16], whereas PL quenching corresponds to exciton decay.

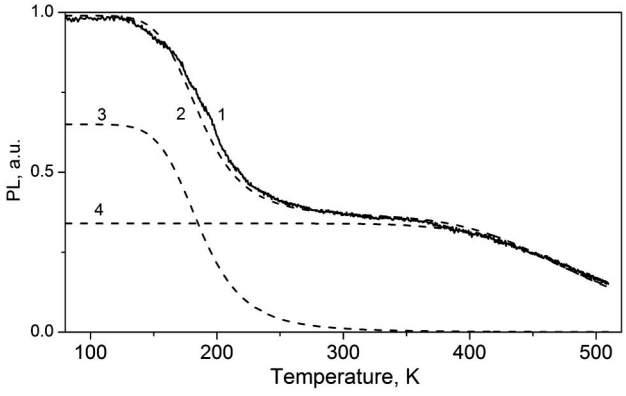

Fig. 4. Temperature dependence of the 2–3 eV PL emission in α-$LiIO_3$ at 3.37 eV excitation: experimental data (curve 1) and data calculated in accord with Mott's law (curve 2). Two individual components (curve 3) and (curve 4) have the pre-exponential factors $4 * 10^4$ and $2 * 10^4$ and thermal activation energies of 0.18 and 0.42 eV, respectively. The heating rate was $\beta \sim 0.2$ K/s.

D. Thermoluminescence

The TL curve for α-$LiJO_3$, recorded after preliminary low-temperature illumination with the 4.2 eV light (300 nm) is given in Fig. 5. Such excitation corresponds to band-to-band transitions in α-$LiJO_3$ and generates free charge carriers, which then are captured by the traps (shallow capture centers). One can see that there are two main types of traps in α-$LiIO_3$, responsible for peaks at 110 and 162 K in TL glow curves, their FWHM being 22 and 30 K, respectively. The shape of the TSL peak is described rather well by the following equation [17]:

$$I(t) = n_0 s \cdot \exp(-E/kT) \cdot \exp\left[-(s/\beta)\int_{T_0}^{T} \exp(-E/k\theta)\mathrm{d}\theta\right], \quad (3)$$

where n_0 is the initial concentration of electrons captured by the traps, s is the effective frequency factor, β is the rate of linear heating (K/s), k is Boltzmann's constant, E is the energy of thermal activation (eV), and T_0 is the initial temperature. The results of TL simulation are shown by solid lines in Fig. 5. Fine solid lines show results of TL simulation in accord with Eq. (3) for peaks at 110 and 162 K, whereas a thick solid line is the sum of two individual components. The experimental TL glow curve agrees well with the calculated curve of the following kinetic parameters: thermal activation energies $E = 0.14$ and 0.21 eV, frequency factors $5 \cdot 10^4$ and 10^4 s^{-1} for peaks at 110 and 162 K, respectively. One can see that there is some difference in the range near 130 K, between the peaks. Maybe there is an additional weak peak from another (third) trap. Charge carriers when captured by the trap may absorb incident light, and crystal demonstrates a photo-induced absorption (PIA) in such a case: samples become darker after shortwave illumination. Because there are only low-temperature TL peaks in Fig. 5, charge carriers are captured only at temperatures below 180 K, and it is only in this temperature range that PIA takes place in α-$LiIO_3$. Thus, there is no PIA in α-$LiIO_3$ at room temperature at which nonlinear converters are used in laser schemes. A specific feature of glow curves in α-$LiIO_3$ is the great number of short-term spontaneous flashes of emission at $T < 170$ K, which superimpose

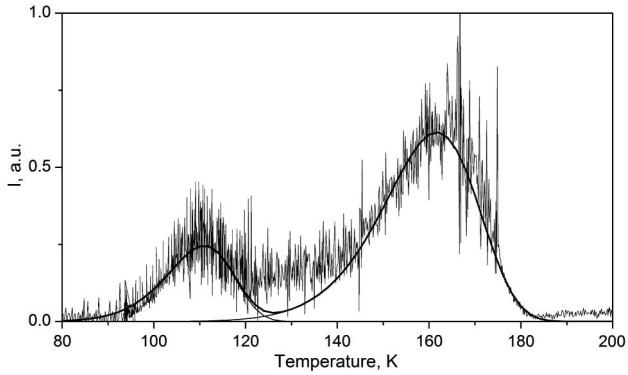

Fig. 5. Glow curve of TL in α-$LiIO_3$ after excitation with the 4.2 eV light (300 nm band-to-band transition) at 80 K. Fine solid lines show results of TL calculation for peaks 110 and 162 K in accord with Eq. (3) [15]; the thick solid line shows the sum of two calculated components.

the usual smooth glow curve, typical of the TL process (Fig. 5). The intrinsic noise of the setup is rather low, as one can see at $T > 170$ K in Fig. 5. These spontaneous flashes correspond to the pyroluminescence in α-$LiIO_3$, which is described in detail in the following section.

E. Spontaneous Emission in α-$LiIO_3$—Pyroelectric Luminescence

When studying the nonisothermic (heating or cooling) processes in α-$LiIO_3$, we discovered its ability to produce a spontaneous pulsed emission [7]. The temperature or temporal dependence of such emission in α-$LiIO_3$ is shown in Fig. 6. One can see that this emission takes place only in a specific temperature range—below 200 K.

This effect has been found in a whole set of molecular organic crystals [8] and later also in some inorganic crystals used in nonlinear optics: KDP [18], triglycine sulfate $(NH_2CH_2COOH)_3 \cdot H_2SO_4$ [19], proustite Ag_3AsS_3 and pyrargyrite Ag_3SbS_3 [20], beta barium borate BBO [21], and lithium metagermanate Li_2GeO_3 [22]. A common feature of these crystals is that they are all pyroelectrics. This emission was called PEL or pyroluminescence [8]. A pyroelectric crystal is characterized by a unit cell with a net dipole moment, and, unlike a ferroelectric, the direction of the resulting lattice polarization cannot be changed by an external electric field. Heating or cooling of such a crystal induces polarization inside until the charge distribution again reaches equilibrium. During this time, the magnitude of the resulting electric fields may be rather large to produce dielectric breakdown. Temperature ranges, where PEL is observed, correlate very well with structural transformations in crystals. Thus, in proustite, PEL is observed in the 20 to 40 K range and near 70 K, which correlates with phase transitions of the II and I types, respectively [20]. In triglycine sulfate, PEL takes place near 322 K, which corresponds to the phase transition of the order–disorder type [19]. In the same temperature ranges, there are also well-pronounced maxima in temperature dependence of pyroelectric coefficients γ [19,20]. The emission flashes are accompanied by simultaneous current pulses [8,22].

The main peculiarities of PEL in α-$LiIO_3$ are the following:

1. PEL intensity lowers as the size of the pyroelectric crystals decreases. PEL disappears completely when the crystal size becomes smaller than 1 mm.
2. The intensity and frequency of PEL depend considerably on the rate of temperature increase or decrease $\beta = dT/dt$. They decrease as an absolute value of β falls.
3. The temperature range where PEL takes place in α-$LiIO_3$ corresponds to maximum γ values (Fig. 6, curve 3). Thus, at 140 K, the pyroelectric coefficient $\gamma = 5 \times 10^{-5}$ coulomb/$m^2 *$ K, which is five times higher than at room temperature [23]. Special measurements show that PEL takes place also near 570 K, which corresponds to a sharp γ maximum in the $\alpha \rightarrow \beta$ phase transition [1].
4. X rays and photoexcitation directly during heating or cooling or at low temperature before heating (the TL regime) suppress PEL up to complete disappearance. Simultaneously, the temperature range where PEL takes place may become narrower.
5. The character of light flashes depends considerably on the crystal plate orientation relative to the optical axis $\boldsymbol{c}$. We studied polished (100) and (001) plates 5 mm × 5 mm × 1 mm in size. In (100), the plate small side faces were perpendicular or along $\boldsymbol{c}$. The character, frequency, and intensity of light flashes were different when one observed PEL in directions perpendicular to $\boldsymbol{c}$ or along $\boldsymbol{c}$. (See Figs. 6a and b, respectively.) It is obvious that in the first case, PEL flashes are casual and occur at $T < 190$ K. In the other case, emission along $\boldsymbol{c}$ is somewhat regular but the temperature range is narrower ($T < 180$ K). In case a, flashes follow very often and superimpose each other: as a result there is some continuous background in the PEL emission. Conversely, there is no background between the rare flashes in case b.

Estimations of the pyroelectric field intensity give values up to 10^6 V/cm: as a result, electric breakdown on the crystal surface or in the volume occurs [8,21]. Because PEL intensity is rather high, one can use it as a sensitive instrument to reveal structural transformations in crystal lattice. But it is necessary

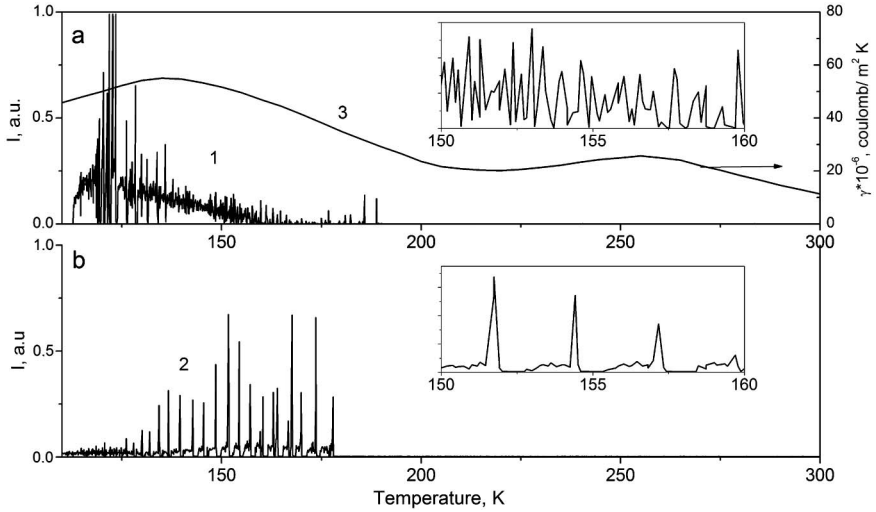

Fig. 6. Spontaneous emission from the (100) α-$LiIO_3$ plate, at observation in the direction a, perpendicular to the optical axis or b, along it, on heating with the $\beta = 0.2$ K/s rate. Curve 3 shows the temperature dependence of the pyroelectric coefficient γ in α-$LiIO_3$ measured with a 2 orders' lower heating rate [22]. Insets, details of PEL temperature dependence for cases a and b.

to take into account that there are other factors that also affect its parameters considerably. If the crystal resistance falls because of electron–hole processes or ionic conductivity, there may be a rapid charge compensation and PEL disappears. It is for this reason that PEL disappears at simultaneous or after preliminary shortwave illumination with $h\nu > 3.3$ eV. In these cases, the resistance lowering is due to the generation of free charge carriers (most effectively, at simultaneous illumination) or to some hopping conductivity along filled traps after preliminary excitation. The wave functions of shallow traps with $E \sim 0.1$–0.2 eV are relatively diffuse and can overlap.

PEL quenching at temperatures above 200 K is partly due to rapid increase of ionic conductivity in α-$LiIO_3$ in this range as temperature grows [4]. Main charge carriers responsible for conductivity increase are interstitial Li^+ ions and Li vacancies, moving along the structural helical channels directed along the ***c*** axis [24].

It is important to understand where the dielectric breakdown takes place: on the crystal surface or inside the crystal. Some authors note that the PEL character depends on gas pressure outside the crystal [17], which indicates the surface process. In this case, we have a discharge in gas or in vacuum and the corresponding emission spectrum is expected to contain a great amount of narrow lines that cover all UV, visible, to near-IR range. However, nobody recorded the PEL emission spectrum to confirm this version spectroscopically to date. On the other hand, a set of experimental facts indicates that PEL occurs also in the crystal volume and includes recombination process inside the pyroelectric crystal, including the polarization of the PEL emission, corresponding to crystal symmetry [18], the slow decay component [8], and only the red component in the PEL spectrum of strongly colored proustite [20], among others.

In our experiments, an internal character of the dielectric breakdown in α-$LiJO_3$ is confirmed also by the following results:

1. We covered the whole α-$LiIO_3$ crystal by a transparent highly conductive film of colloidal silver. Suppose that the pyrocharge concentrates only on the crystal surface, the charge as well as the PEL disappears rapidly because of the high conductivity along the conductive film. We found that the PEL intensity from coated α-$LiIO_3$ crystal decreased, but the PEL effect itself remained, and we observed the light flashes both at heating and cooling.
2. The orientation effect takes place for PEL. The character of temporal or temperature dependence and the emission intensity is considerably differently, depending on the direction along which PEL is recorded: along [010] or along [001]. Typical PEL patterns are shown in Figs. 6a and 6b, respectively.

To understand the reasons of PEL anisotropy, it is worth remembering that there is a strong anisotropy also in the electrical conductivity of the α-$LiIO_3$ crystals [4–6]. It was established that conductivity in the direction perpendicular to optical axis ***c*** was of about $10^{-11} \div 10^{-12}$ $ohm^{-1}cm^{-1}$ and did not depend on the acidity (pH) of the mother solution during growth, whereas along ***c*** the conductivity magnitude varied from 10^{-5} to 10^{-11} ($ohm^{-1}cm^{-1}$) [5–6]. This anisotropy is explained as a result of the presence of channel defects directed along ***c*** in the α-$LiIO_3$ samples [5–6]. According to these authors, channel defects exist practically in all α-$LiIO_3$ samples, but in most cases they are of submicrometer sizes and are invisible for conventional optical microscopy. However, a special ultrasonic treatment in the electric field allowed us to increase their size (for example, up to diameter of 10 μm) and make them visible. Patterns demonstrating channel defects in α-$LiIO_3$ after such treatment are given in Figs. 7 and 8.

These channels in α-$LiIO_3$ may be empty [25] or filled with a mother solution [4–6]. The authors of [5–6] suppose that the electrical conductivity along the mother solution in filled channels is responsible for the conductivity anisotropy. We suppose that the observed PEL anisotropy at $T < 200$ K is a result of the electric breakdown inside such channel defects when fluid inside the channels is frozen and operates as a dielectric. Because the refractive index in channels is somewhat below that in the α-$LiJO_3$ lattice and because of multiple internal reflections, the PEL emission propagates mainly along the linear channels, as in the case of optical fibers. When observing PEL along the direction perpendicular to the ***c*** axis, we record mainly emission resulting from breakdowns in the crystal volume around channels. Thus, the PEL anisotropy in α-$LiIO_3$ crystals is a result of the presence of channel-type extended defects. The PEL quenching as temperature increases in α-$LiIO_3$ is a combined effect both of a decrease in the pyrocoefficient γ (Fig. 6) and the growth of crystal conductivity, mainly along channels. Features in the 100 to 200 K temperature range were found in α-$LiIO_3$ also in temperature dependence of the acoustic speed and of absorption of longitudinal ultrasonic waves passing along the ***c*** axis as well as in the relaxation of the electroacoustic echo [4].

In nonlinear laser devices, the intensity of pumping light is normally very high and local heating because of residual absorption is possible. In this case, a strong pyroelectric field appears in the lattice of the pyroelectric nonlinear converter. Dielectric breakdown is considered one of the possible mechanisms of nonlinear crystal damage [21]. From this point of

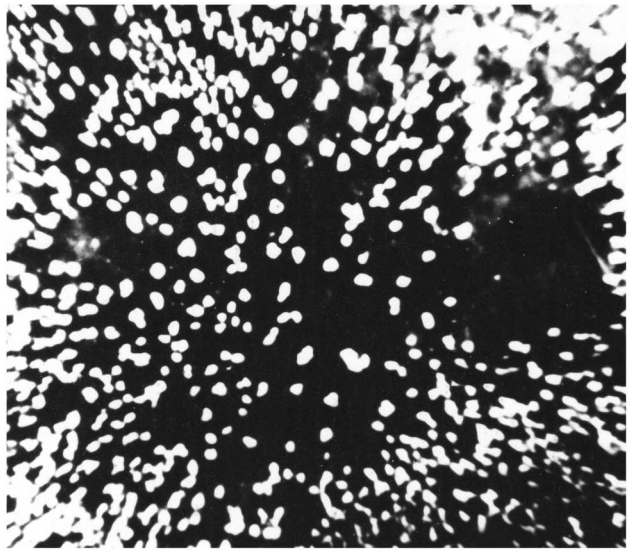

Fig. 7. Distribution pattern of etching pits (exits of the channels) under electrodes after combined current and ultrasonic treatment of (001) α-$LiIO_3$ plate. Magnification, ×150.

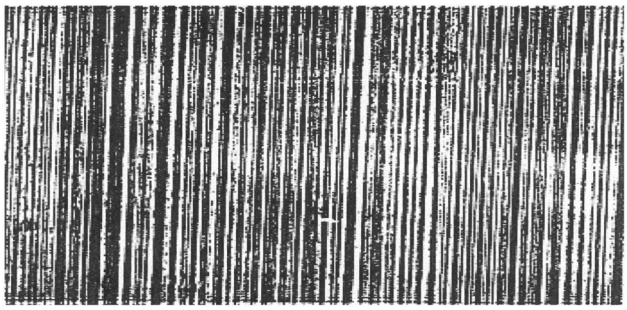

Fig. 8. Shadow pattern demonstrating current damage in the α-$LiJO_3$ sample. The cross-hatching direction is along the ***c*** axis. Magnification, ×150.

view, PEL quenching above 200 K in α-$LiJO_3$ promotes an increase of its optical damage threshold at room temperature at which the crystal operates in laser devices [2]. It is noteworthy that we found channel defects in many other nonlinear crystals such as potassium pentaborate KB5, KTP, BBO, and LBO, which also demonstrate the PEL effect. Thus, the features that we observed in α-$LiIO_3$ may be common for different nonlinear crystals both organic and inorganic.

4. CONCLUSIONS

Broadband PL with two main components at 2.95 and 2.6 eV was found in nonlinear lithium iodate α-$LiIO_3$ crystals with the 4.37 eV bandgap. The low-temperature 2.95 eV emission excited in the 4.3 eV band, near the fundamental absorption edge, with a large Stokes shift, is associated with STEs. The 2.6 eV emission excited in broad bands at 3.25 and 3.95 eV is related to oxygen vacancies (F-centers). The PL of STEs quenches to 250 K with activation energy $\Delta E = 0.18$ eV as temperature increases, whereas the F-center PL quenches considerably slower ($\Delta E = 0.42$ eV). Free charge carriers may be captured by two types of shallow traps with thermal activation energies of 0.14 and 0.21 eV, which at room temperature are empty and do not reduce to photoinduced darkening of the nonlinear α-$LiIO_3$ converters. In the nonisothermic regime, strong pyroelectric fields with intensity $\sim 10^6$ V/cm appear in the α-$LiIO_3$ lattice, which results in spontaneous electric breakdowns accompanied by the simultaneous light flashes on the crystal surface and in its bulk. PEL emission is a sensitive indicator of crystal lattice transformations as temperature changes. Analysis of PEL temporal and temperature dependence indicates that breakdowns occur both inside channel defects and around them.

ACKNOWLEDGMENTS

This work was supported partly by a grant from the Russian Foundation for Basic Research (RFBR, grant no. 11-02-00817a).

REFERENCES

1. K. I. Avdienko, S. V. Bogdanov, S. M. Arkhipov, B. I. Kidyarov, V. V. Lebedev, Yu. E. Nevsky, V. I. Trunov, D. V. Shelaput, and R. M. Shklovskaya, *Lithium Iodate: Growth, Properties and Application* (Nauka, 1980), p. 144.
2. D. N. Nikogosyan, *Nonlinear Optical Crystals: A Complete Survey* (Springer, 2005), p. 428.
3. S. Matsumura, "Polymorphism of lithium iodate," Mater. Res. Bull. **6**, 469–477 (1971).
4. A. A. Blistanov, *Crystals of Quantum and Nonlinear Optics* (MISIS, 2000), p. 432.
5. L. I. Isaenko, I. F. Kanaef, V. K. Malinovsky, and V. I. Tyurikov, "Macroscopic channel structures in α-$LiIO_3$," Phys. Solid State **30**, 348–360 (1988).
6. V. I. Tyurikov, "Growth channel microdefects in single crystals of lithium iodate and their effect on crystal physical properties," Ph.D. thesis (Siberian Branch of Russian Academy of Sciences, 2001).
7. A. P. Yelisseyev, L. I. Isaenko, and G. L. Noskov, "Luminescence features of lithium iodate," Autometry **4**, 112–114 (1988).
8. J. S. Patel and D. M. Hanson, "Pyroelectric luminescence," Nature **293**, 445–447 (1981).
9. G. C. Bhar and R. C. Smith, "Optical properties of II-IV-V_2 and I-II-VI_2 crystals with particular reference to transmission limits," Phys. Status Solidi A **13**, 157–168 (1972).
10. T. S. Moss, *Optical Properties of Semiconductors* (Butterworth, 1961).
11. J. M. Crettez, J. Comte, and E. Coquet, "Optical properties of α and β lithium iodate in the visible range," Opt. Commun. **6**, 26–29 (1972).
12. B. H. T. Chai, Optical Crystals, in *CRC Handbook of Laser Science and Technology: Supplement 2: Optical Materials*, M. J. Weber, ed. (CRC Press, 1995).
13. M. K. Rodionov, N. P. Evtushenko, M. F. Koldobskaya, and V. V. Alexeev, "IR absorption and reflection spectra of lithium iodate," Ukr. J. Phys. **50**, 804–810 (1980, in Russian).
14. A. Yu. Klimova, A. F. Konstantinova, Z. B. Perekalina, N. A. Baturin, and G. F. Dobrzhansky, "The effect of growth conditions on optical properties of crystals of composition $LiIO_3$-HIO_3," Crystallogr. Rep. **28**, 1191–1196 (1983).
15. T. V. Perevalov, O. E. Tereshenko, V. A. Gritsenko, V. A. Pustovarov, A. P. Yelisseyev, C. Park, J. H. Han, and C. J. Lee, "Oxygen deficiency defects in amorphous Al_2O_3," J. Appl.Phys. **108**, 013501 (2010).
16. K. S. Song and R. T. Williams, *Self-Trapped Excitons*, Vol. XII (Springer-Verlag, 1993), p. 403.
17. C. Furetta, *Handbook of Thermoluminescence* (World Scientific, 2003), p. 461.
18. H. P. Yockey and C. L. Aseltine, "Development of high voltages in potassium dihydrogen phosphate irradiated by γ rays," Phys. Rev. B **11**, 4373–4382 (1975).
19. F. Jaque, J. M. Herreros, and C. Sanchez, "Thermally excited light emission from triglycine sulfate (T.G.S.)," Solid State Commun. **12**, 63–66 (1973).
20. S. L. Bravina, A. K. Kadaschuk, N. V. Morozovsky, N. I. Ostapenko, Yu. A. Skryshevsky, and M. T. Shpak, "Pyroelectric luminescence of proustite and pyrargyrite," Tech. Phys. **58**, 1404–1406 (1988) (in Russian).
21. V. T. Adamiv, Ya. V. Burak, M. P. Panasyuk, and I. M. Teslyuk, "Pyroelectroluminescence of barium beta borate single crystals," Tech. Phys. Lett. **24**, 62–65 (1998) (in Russian).
22. S. L. Bravina, A. K. Kadaschuk, N. V. Morozovsky, N. I. Ostapenko, and Yu. A. Skryshevsky, "Pyroelectric effect in metagermanate lithium," Tech. Phys. **60**, 97–101 (1990) (in Russian).
23. A. S. Bhalla, "Low temperature pyroelectric properties of α-$LiIO_3$ single crystals," J. Appl. Phys. **55**, 1229–1230 (1984).
24. M. Remoissenet, J. Garandet, and H. Arend, "Influence of crystal growth conditions on electrical properties and phase transitions in $LiIO_3$," Mater. Res. Bull. **10**, 181–185 (1975).
25. L. V. Atroshenko, Ya. A. Obukhovsky, and N. V. Khodeea, "The etching features of α-$LiIO_3$ single crystals," Crystallogr. Rep. **22**, 414–416 (1977).